UNIVERSITY OF CALIFORNIA, SAN DIEGO

UCSD

BERKELEY • DAVIS • LOS ANGELES • RIVERSIDE • SAN DIEGO • SAN FRANCISCO   SANTA BARBARA • SANTA CRUZ

SCRIPPS INSTITUTION OF OCEANOGRAPHY

LA JOLLA, CALIFORNIA 92093

28 August, 1996

Dr. James C. Dodge
National Aeronautics and Space Administration
Earth Science and Applications Division
Office of Space Science and Applications
NASA Headquarters
300 E Street SW
Washington, DC 20546

Subject: **Final Report for NASA Grant NAGW-2964 "Analysis of Long-Term Cloud Cover, Radiative Fluxes, and Sea Surface Temperature in the Eastern Tropical Pacific" J.J. Simpson, Principal Investigator and R. Frouin, Associate Investigator.**
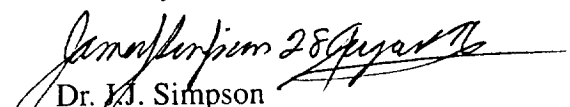
Dear Dr. Dodge:

This final report documents work accomplished during the project "Analysis of Long-Term Cloud Cover, Radiative Fluxes, and Sea Surface Temperature in the Eastern Tropical Pacific", NASA Grant # NAGW2964, J.J. Simpson, Principal Investigator, R. Frouin, Associated Investigator.

The contributions of the Principal Investigator (J. Simpson) are reported under four (4) categories: 1) AVHRR Data; 2) GOES Data; 3) System Software Design; and 4) ATSR Data. The contributions of the Associate Investigator (R. Frouin) are reported for: 1) Longwave Irradiance at the Surface; 2) Methods to Derive Surface Short-wave Irradiance; and 3) Estimating PAR at the Surface. Several papers have resulted. Abstracts for each paper and its current status (e.g., submitted, in press, published) are provided. Only representative results for papers as yet unpublished are attached.

Thank you very much for your continued encouragement and support throughout the project. I hope we'll be able to work together again in the near future.

Sincerely,

Dr. J.J. Simpson
Principal Investigator

cc: R. Frouin

CONTRIBUTIONS OF PRINCIPAL INVESTIGATOR

I. AVHRR RELATED WORK

A. Reduction of Noise in AVHRR Channel 3 Data with Minimum Distortion.
J.J. Simpson and S.R. Yhann, 1994
IEEE Transactions on Geoscience and Remote Sensing, 32: 315-328.

ABSTRACT

The channel 3 data of the Advanced Very High Resolution Radiometer (AVHRR) on the NOAA series of weather satellites (NOAA 6-14) are contaminated by instrumentation noise. The signal to noise ratio (S/N) varies considerably from image to image and the between sensor variation in S/N can be large. The characteristics of the channel noise in the image data are examined using Fourier techniques. A Wiener filtering technique is developed to reduce the noise in the channel 3 image data. The noise and signal power spectra for the Wiener filter are estimated from the channel 3 and channel 4 AVHRR data in a manner which makes the filter adaptive to observed variations in the noise power spectra. Thus, the degree of filtering is dependent upon the level of noise in the original data and the filter is adaptive to variations in noise characteristics. Use of the filtered data to improve image segmentation, labeling in cloud screening algorithms for AVHRR data, and multichannel sea surface temperature (MCSST) estimates is demonstrated. Examples also show that the method can be used with success in land applications. The Wiener filtering model is compared with alternate filtering methods and is shown to be superior in all applications tested.

B. Application of Neural Networks to AVHRR Cloud Segmentation
S.R. Yhann and J.J. Simpson, 1995
IEEE Transactions on Geoscience and Remote Sensing, 33: 590-604.

ABSTRACT

The application of neural networks to cloud screening of AVHRR data over the ocean is investigated. Two approaches are considered, interactive cloud screening and automated cloud screening. In interactive cloud screening a neural network is trained on a set of data points which are interactively selected from the image to be screened. Because the data variability is limited within a single image, a very simple neural network topology is sufficient to generate an effective cloud screen. Consequently, network training is very quick and only a few training samples are required. In automated cloud screening, where a general network is designed to handle all images, the data variability can be significant and the resulting neural network topology is more complex. The latitudinal, seasonal and spatial dependence of cloud screening large AVHRR data sets is studied using an extensive data set spanning 7 years. A neural network and associated feature set are designed to cloud screen this data set. The sensitivity of the thermal infra-red bands to high atmospheric water vapor concentration was found to limit the accuracy of cloud screening methods which rely solely on data from these channels. These limitations are removed when the visible channel data is used in combination with the thermal infra-red data. A post processing algorithm is developed to improve the cloud screening results of the network in the presence of high atmospheric water vapor concentration. Post processing also is effective in identifying pixels contaminated by sub-pixel clouds and/or amplifier hysteresis effects at cloud-ocean boundaries. The neural network, when combined with the post processing algorithm, produces accurate cloud screens for the large, regionally distributed AVHRR data set.

C. Improved Cloud Detection for Daytime AVHRR Scenes over Land
J.J. Simpson and J.I. Gobat, 1996
Remote Sensing of the Environment, **55**: 21-49.

ABSTRACT

Accurate cloud detection in Advanced Very High Resolution Radiometer (AVHRR) data over land is a difficult task complicated by spatially and temporally varying land surface reflectances and emissivities. The AVHRR Split-and-Merge Clustering (ASMC) algorithm for cloud detection in AVHRR scenes over land provides a computationally efficient, scene specific, objective way to circumvent these difficulties. The algorithm consists of two steps: 1) a split-and-merge clustering of the input data (calibrated channel 2 albedo, calibrated channel 4 temperature, and a channel 3 - channel 4 temperature difference) which segments the scene into its natural groupings; and 2) a cluster labelling procedure which uses scene specific, joint three-dimensional adaptive labelling thresholds (as opposed to constant static thresholds) to label the clusters as either cloud, cloud-free land, or uncertain. The uncertain class is used for those pixels whose signature is not clearly cloud-free land or cloud (e.g., pixels at cloud boundaries which often contain subpixel cloud and land information which has been averaged together by the integrating aperture function of the AVHRR instrument). Results show that the ASMC algorithm is neither regionally nor temporally specific and can be used over a large range of solar altitudes. Sensitivity of the segmentation and labelling steps to the choice of input variables also was studied. Results obtained with the ASMC algorithm also compare favorably with those obtained from a wide range of currently used algorithms to detect cloud over land in AVHRR data. Moreover, the ASMC algorithm can be adapted for use with data to be taken by the Moderate Resolution Imaging Spectrometer-Nadir (MODIS-N).

D. Multivariate Alteration Detection (MAD) and MAF Post-Processing in Multi-spectral, Bi-temporal Image Data: New Approaches to Change Detection Studies
A.A. Nielsen, K. Conradsen, and J.J. Simpson, 1996
Submitted to *Remote Sensing of Environment*

ABSTRACT

Accurate and quantitative change detection in a temporal sequence of satellite scenes is an important requirement for many climate and global change studies. This paper uses two multivariate statistical transformations (the Minimum/Maximum Autocorrelation Factors (MAF) transformation and the Multivariate Alteration Detection (MAD) transformation) to quantitatively and accurately detect changes in sequences of satellite data. Both Landsat Multispectral Scanner System (MSS) data and Advanced Very High Resolution Radiometer (AVHRR) data, together with the above cited analysis methods, are used to quantify case studies of: 1) urbanization; and 2) ENSO-related alteration of ocean thermal structure. Change detection measures also are computed using the popular Principal Component Transformation (PCT). These latter analyses are compared with those derived using the MAF/MAD analyses. The MAF/MAD analysis is less effected by noise in the data than is the PCT analysis and the MAF/MAD analysis also is more effective than PCT analysis for the detection of outliers in data. Results show that the MAF/MAD transformation is preferred to the PCT analysis under circumstances in which calibration is uncertain or time varying.

E. An Improved Fuzzy Logic Segmentation of Sea Ice, Clouds and Ocean in Remotely Sensed Arctic Imagery
J.J Simpson and R.H. Keller, 1995
Remote Sensing of Environment, 54: 290-312
ABSTRACT

The accurate segmentation of sea ice from cloud and from cloud-free ocean in polar AVHRR imagery is important for many scientific applications (e.g., sea ice - albedo feedback mechanisms, heat exchange between ocean and atmosphere in polar regions, studies of the stability of surface water in polar regions). Unfortunately, it is a difficult task complicated by the common visible reflectance characteristics of sea ice and cloud. Moreover, AVHRR channel 3 data historically have been contaminated by highly variable sensor noise which generally has hampered their use in the classification of polar scenes. Likewise, polar scenes often contain pixels with mixed classes (e.g., sea ice and cloud). This paper uses a combination of fuzzy logic classification methods, noise reduction in AVHRR channel 3 data using Wiener filtering methods (Simpson and Yhann, 1994), and a physically motivated rule base which makes effective use of the Wiener filtered channel 3 data to more accurately segment polar imagery. The new method's improved classification skill compared to more traditional methods, as well as its regional independence, is demonstrated. The algorithm is computationally efficient and hence is suitable for analyzing the large volumes of polar imagery needed in many global change studies.

F. A Procedure for the Detection and Removal of Cloud Shadow from AVHRR Data over Land
J.J. Simpson and J.R. Stitt, 1996
Submitted to *Remote Sensing of Environment*
ABSTRACT

Although the accurate detection of cloud shadow in AVHRR scenes is important for many terrestial applications (e.g., accurate biome boundary detection from normalized vegetation index (NDVI) maps), relatively little work in this area has appeared in the literature. This paper presents a new algorithm for cloud shadow detection for use with AVHRR daytime scenes over land. The procedure consists of five steps and starts with accurate cloud detection in the scene using the AVHRR Split-and-Merge Clustering algorithm developed by Simpson and Gobat (1996). Then, the procedure uses a combination of geometric and optical constraints derived from the pixel by pixel cross track geometry of the scene and morphological image transformations to accurately detect cloud shadow. The results show that the procedure works well in tropical and mid-latitude regions under varying atmospheric conditions (wet-dry) and with different types of terrain. The method is not intended for use in polar regions or under conditions of poor solar illumination. Moreover, the method can be adapted for use with Landsat and Moderate Range Imaging Spectrometer-N (MODIS-N) data. An example of the effectiveness of the method is shown in Figure 1.

G. Improved Estimates of the Areal Extent of Snow Cover from AVHRR Data

J.J. Simpson, J.R. Stitt, and M. Sienko, 1996

ABSTRACT

Satellite data provide the only practical way to obtain the necessary spatial and temporal coverage of areal extent of snow cover required to produce accurate estimates of snow water equivalents. Unfortunately, the accurate separation of snow cover from cloud cover in visible and thermal satellite data (e.g., the Advanced Very High Resolution Radiometer (AVHRR)) is a difficult task complicated by: 1) the similar reflectivities of snow cover and cloud cover in the visible region of the spectrum; 2) partial overlap in the thermal signature of clouds and snow, especially between warm, low clouds and snow; and 3) highly variable background reflectances and emissivities of the land surfaces on which snow can accumulate. A multi-spectral, multi-stage snow detection (MSSD) procedure has been developed which: 1) accurately separates snow and cloud from clear land in a terrestial scene; and 2) uses other criteria to separate both cold, high clouds and warm, low clouds from snow. A mixed pixel class also is identified and pixels in this class can be assigned a percentage composition (cloud, snow, land) using a linear mixing model. The procedure has been ground-truthed with both Landsat data and with SNOTEL (SNOwTELemetry) observations. Classification skill, based on a statistical comparison with SNOTEL observations, is about 97%. Application of the procedure to a wide variety of terrestial environments is demonstrated. Because of its classification skill, objective nature, and computational efficiency, it will be used by the National Weather Service operationally starting October 1996. The improved estimates of areal extent of snow cover (and hence snow water equivalent estimates) also should prove useful to hydrometeorological programs such as the Global Energy and Water Cycle Experiment (GEWEX). An example of the classification with accompanying SNOTEL data is given in Figure 2.

H. Spatial Degradation of Satellite Data and its Effects on Accurate Cloud Detection over the Ocean

J.J. Simpson, S.A. Cowley, and R.H. Keller, 1996

ABSTRACT

A study of the effects of the spatial degradation of satellite data on cloud detection schemes was performed. Results from full resolution analyses were compared with 9 commonly used GAC processing scenes. Results also were compared with 50 years of shipboard observations off the west coast of the United States and Canada. The results show that several commonly used GAC procedures do not faithfully represent cloud cover when compared either the shipboard data or with results using the same cloud detection algorithm but on full resolution satellite data. Comparison (Figure 3) among our full resolution results, the 50 year shipboard cloud climatology, and results for the region produced by the International Satellite Cloud Climatology Project (ISCCP) show that our full resolution results are consistent with the shipboard climatology whereas those of ISCCP: 1) fail to reproduce seasonal variation in cloud cover for the region; and 2) significantly overestimate cloud cover compared to the shipboard values.

II. GOES RELATED WORK

A. Improved Destriping of GOES Data Using Finite Impulse Response Filters
J.J. Simpson, J.I. Gobat, and R. Frouin, 1995
Remote Sensing of the Environment, 52: 15-35.
ABSTRACT

GOES data are known to be contaminated with stripes whose presence affects the usefulness of the data in quantitative studies. This research: 1) reviewed the causes of the striping; 2) developed frequency domain and spatial domain finite impulse response (FIR) filters for minimizing the stripes in the data while simultaneously introducing minimum distortion into the filtered data; and 3) quantitatively compared the results obtained with these new filtering methods with those produced by traditional destriping methods (e.g., simple smoothing, moment matching, histogram matching). Results from 81 GOES scenes show that a finite impulse response filter (i.e., target filter), implemented in either the spatial or Fourier domain, is superior to all other methods evaluated. The importance of proper destriping of GOES data for both accurate cloud detection and radiative flux computations also is demonstrated. The sensitivity of histogram matching to the choice of reference state is evaluated and a way to minimize the sensitivity is presented.

B. Improved Cloud Detection in GOES Scenes over Land
J.J. Simpson and J.I. Gobat, 1995a
Remote Sensing of the Environment, 52: 36-54.
ABSTRACT

Accurate cloud detection in satellite data over land is a difficult task complicated by spatially and temporally varying land surface reflectivities and emissivities. The GOES Split-and-Merge Clustering (GSMC) algorithm for cloud detection in GOES scenes over land provides a computationally efficient, scene specific way to circumvent these difficulties. The algorithm consists of three steps: 1) a split-and-merge clustering of the input data which segments the scene into its natural grouping; 2) a cluster labeling procedure which uses scene specific adaptive thresholds (as opposed to constant static thresholds) to label the clusters as either cloud or cloud-free land; and 3) a post-processing step which imposes a degree of spatial uniformity on the labeled land and cloud pixels. An "a priori" mask feature also enhances cloud detection in traditionally difficult scenes (e.g., clouds over bright desert). Results show that the GSMC algorithm is neither regionally nor temporally specific and can be used over a large range of solar altitudes.

C. Improved Cloud Detection in GOES Scenes over the Ocean
J.J. Simpson and J.I. Gobat, 1995b
Remote Sensing of the Environment, 52: 79-94.
ABSTRACT

Accurate cloud detection in GOES data over the ocean is a difficult task complicated by poor spatial resolution (4 km) in the GOES IR data, relatively coarse quantization (6 bits) for GOES VIS data, a visible sensing region of the spectrum not ideally suited for cloud vs. ocean segmentation, and relatively small oceanic signal dynamic range compared to that of either cloud or land structures found in a typical GOES scene. The GOES Adapted LDTNLR Ocean Cloud

Mask (GALOCM) algorithm for cloud detection in GOES scenes over the oceans provides a computationally efficient, scene specific way to circumvent these difficulties. The algorithm consists of four steps: 1) generate a cloud mask using the Local Dynamic Threshold Non-Linear Rayleigh (LDTNLR) algorithm of Simpson and Humphrey (1990); 2) generate a second cloud mask using an adaptive threshold; 3) divide the pixels in the scene into three groups (both methods agree pixel is ocean, is cloud, or the pixel is in contention); and 4) iteratively apply an adaptive threshold to the contested pixels. Convergence occurs when pixels are no longer in contention based on statistical criteria. Results show that the GALOCM method produces accurate cloud masks over the oceans which are neither regionally-dependent nor temporally specific. GOES scenes containing ocean, cloud and land are best cloud screened using a combination of the GOES Split-and-Merge Clustering (Simpson and Gobat, 1995a) and the GALOCM algorithms.

D. Radiometric Calibration of GOES-7 VISSR Solar Channels during the GOES Pathfinder Benchmark Period
R. Frouin and J.J. Simpson, 1995
Remote Sensing of the Environment, 52: 95-115
ABSTRACT

The GOES-7 VISSR solar channels are radiometrically calibrated for the period from June 1987 through November 1988. Space, White Sands, and the Sonora Desert are used as calibration targets. The calibration is performed in three different ways: 1) using the stretched data (i.e., retransmitted data operationally destriped using NOAA's normalization procedure) and considering individual VISSR detectors separately; 2) using the stretched data averaged over the 8 VISSR detectors; and 3) using the stretched data further destriped according to Simpson et al., (1995) and then averaged over the 8 VISSR detectors. The third approach provides the best results (i.e., best equalization of the detectors). Because of uncertainties in the modeling of the VISSR radiance, using separate calibration coefficients for each detector (first approach) may not reduce the striping significantly. The calibration coefficients exhibit low frequency changes (about 40% of the mean values over the study period) which are not correlated with seasonal variations in the extra-terrestrial solar irradiance. High frequency fluctuations (over a few days) are large, and they are due in part to NOAA's normalization procedure and to calibration uncertainties. Differences between the calibration coefficients of individual detectors also are large, as well as changes between consecutive VISSR acquisition times. Comparison of untampered (retransmitted data but not operationally destriped using NOAA's normalization procedure) "Wednesday" 1848 GMT data with stretched 1831 and 1901 GMT data indicates that NOAA's normalization procedure, though imperfect, reduces substantially the stripes present in the data transmitted by the satellite to the NOAA CDA facility in Wallops Island. There is evidence, however, that NOAA's normalization procedure introduced artificial variations in the count squared of the targets that in one instance resulted in 30% lower calibration coefficients. The average calibration coefficients are generally higher by 15% than the values of Rossow et al., (1992); they are in better agreement with the values of Abel et al., (1993) and Whitlock et al., (1994). Because the residual stripes in the data available to the users are highly variable and unpredictable, it is recommended that the radiometric calibration of the VISSR solar channels should be performed as frequently as possible (every day). For best results, average calibration coefficients should be applied to data destriped according to Simpson et al., (1995). Though the stripes in the VISSR data transmitted to Wallops Island should be reduced for operational, real-time purposes (e.g., weather analysis and forecast),

the original unnormalized data should be archived for subsequent use in quantitative, scientific applications.

III. SYSTEM SOFTWARE DEVELOPMENT

A. The Tiling and General Research Imaging System (TIGRIS)
J.J. Simpson and L. Al-Rawi, 1996
IEEE Transactions on Geosciences and Remote Sensing, 34: 149-162

ABSTRACT

The Tile and General Research Imaging System (TIGRIS) is a UNIX-based image software system implemented in, and strictly conforming to, UNIX, C/ANSI C, and X11 Window standards. The TIGRIS design and implementation emulates UNIX at the user, application and system levels. The TIGRIS Application Programmer Interface (API) provides a convenient way to create diverse image processing, analysis, and visualization applications. TIGRIS has been used primarily to support satellite remote sensing, global change research and operational activities. Numerous applications related to specific remote sensing issues (e.g., cloud detection, noise reduction in AVHRR Channel 3 data, oceanic transport) are included in the application layer. In addition, a number of powerful general purpose imaging applications (e.g., image algebra, morphological operations, textural analysis) are provided which support general image processing, analysis, interactive visualization, and non-interactive image product generation.

IV. ATSR

A. Reduction of Clouds in Along Track Scanning Radiometer (ATSR) Data Over the Ocean
J.J. Simpson, A. Schmidt, and A. Harris, 1996
To be submitted to *IEEE Transactions on Geosciences and Remote Sensing*

ABSTRACT

Valid estimates of Sea Surface Temperature (SST) from satellite data (e.g., the Along Track Scanning Radiometer (ATSR)) are critically dependent upon the identification and removal of cloud from the data. Unfortunately, few cloud-screening algorithms for ATSR data have appeared in the literature. A robust, new algorithm for cloud masking has now been developed which is very effective at removing cloud contamination from both the forward and nadir views of ATSR images regardless of cloud type. The method, with evaluates every pixel in the image, is statistically reproducible, computationally efficient, and requires no knowledge of cloud type. Results were validated with buoy observations of SST. For the images tested mean differences (buoy-SST) were + 0.02°C ± 0.43°C. The new procedure also compares favorably with the standard ATSR operational cloud mask product. The algorithm can be used in tropical and midlatitude regions. The algorithm is not designed to detect sea ice, and consequently should not be used in polar regions. Finally, the approach is so general that it can easily be adapted to ATSR-2 data and to other data from soon to be launched sensors (e.g., new AVHRR on NOAA-K, L, M series, AATSR, MODIS), thus making climatological cloud atlases based on various remotely sensed data sets easier to produce, interpret and use. An example is given in Figure 4.

CONTRIBUTIONS OF ASSOCIATE INVESTIGATOR

1. Estimating Longwave Irradiance at the Surface from HIRS/2 Data

We have applied the methodology of Frouin *et al.*, 1988 to HIRS/2 data. Only parameters derived from HIRS/2 data are used in the radiative transfer model, namely cloud top pressure, fractional cover, surface temperature, and vertical profiles of temperature and moisture. These parameters will be derived with improved accuracy in the future, from sensors like AIRS on the EOS PM-1 platform. Since cloud base pressure, a key parameter affecting downward longwave irradiance, is not derived from HIRS/2 data, we deduce it from cloud top pressure assuming a cloud thickness of 50 mb (see Frouin *et al.*, 1988). To compute the upward component, we use a surface emissivity equal to 1. Parameters of secondary importance, such as ozone and carbon dioxide mixing rations, are taken from climatology. The dataset analyzed has been collected in Wisconsin during October-November 1986, for purposes of both cirrus cloud measurements and surface radiation budget algorithm validation activities.

Figure 5 compares estimated and measured downward longwave irradiance at F. McCoy (43.96°, − 97.76°). Large differences exist between estimated and measured values, reaching 100 Wm^{-2} on Julian days 292 and 305. Using 1-, 2-, 5-, 10-, 15-, 30-, or 60-minute averages for the measured values, the rms error does not change significantly; it remains near 51 Wm^{-2} (Fig. 6). HIRS/2 -derived precipitable water is always higher than precipitable water from radiosonde (Fig. 7). The effect is to bias high the downward longwave irradiance estimates, but no systematic effect is observed in Fig. 5. Vertical profiles of temperature from HIRS/2 and radiosonde are generally in agreement (e.g., Fig. 8), but differences of 7K (higher HIRS/2 values occur near the surface on October 15 and 17, 86 (not shown here). The higher HIRS/2 temperature values may partly explain the higher downward longwave irradiance estimates obtained for those days (Fig. 5). Except for October 22, 86, HIRS/2 cloud base is also significantly lower than lidar cloud base (Table 1). Our crude parameterization of cloud base, therefore, does not explain the discrepancy between HIRS/2 cloud base and lidar cloud base.

Figure 9 displays daily averages at 5 stations within the experimental area. The rms error and average difference between estimated and measured values are 35.3 and 21.3 Wm^{-2}, respectively. The rms error is reduced compared to that obtained on an hourly time scale (51 to 35 Wm^{-2}). Applying the algorithm to the entire experimental area, the fields of downward and upward components of longwave irradiance, as well as net irradiance are obtained (Fig. 10a, b, and c). Compared to ECMWF analyses, the HIRS/2-derived fields exhibit more spatial variability, which is expected since the ECMWF resolution is 1.12° x 1.12°. The ECMWF values, however, are higher in magnitude than the HIRS/2-derived values by 30 to 50 Wm^{-2}, especially on October 15, 86.

2. A Review of Satellite Methods to Derive Surface Short-Wave Irradiance

In this study by Pinker, Frouin, and Li (1995), we review progress made during the last decade in satellite methods to derive downward and new surface solar irradiance. We discuss current capabilities and activities, and future needs. Methods for deriving downward surface solar irradiance are becoming operational. They are being used increasingly to address climate issues, such as determining the role of solar forcing in oceanic processes, hydrological modeling, and in carbon cycling. Based on extensive comparisons with ground-truth data, estimates of downward surface solar irradiance can be obtained within 20 Wm^{-2}, or better on monthly time scales, for areas of an average climate model grid size. Methods for deriving the net surface solar irradiance

directly have recently been proposed, but need to be further evaluated.

Several aspects of current satellite methods need to be re-examined, including available information on the state of the atmosphere and the surface, used as input in the models, cloud screening, and more detailed information on cloud types or structure. However, at present it is not clear whether further improvements in the physics of the models alone would improve results. More work is also needed on ground sampling strategies to make satellite validation meaningful. Satellite sensors suitable for surface radiation budget monitoring are not limited to those used so far in algorithm development, i.e., polar and geostationary meteorological satellites. Other sensors, scanners as well as wide field-of view sensors, in particular those from the Earth radiation Budget experiment and the follow-up Clouds and Earth's Radiant Energy System, are suitable tools for studying surface radiation budget's inter-annual variability and issues of climate change.

3. Estimating PAR at the Earth's Surface from Satellite Observations

In this study by Frouin and Pinker (1995), we examined current satellite algorithms to estimate photo-synthetically active radiation (PAR) at the Earth's surface, including the algorithm of Frouin and Gautier (1991). PAR can be obtained directly from top-of-atmosphere solar radiance, which is used to determine atmospheric transmissivity. Since clouds do not absorb significantly at PAR wavelengths, the radiative transfer modeling is generally simplified compared to that of insolation. The accuracies reported, about 10 and 6% on daily and monthly time scales, respectively, are useful for modeling oceanic and terrestrial primary productivity. Improvements are needed, however, in the presence of heterogeneous cloud cover and in the presence of snow and ice. The large scale variability in the ratio of PAR and insolation, essentially due to clouds, is reduced at daily and longer time scales, suggesting that reasonable accurate PAR climatologies can be obtained from available insolation climatologies.

REFERENCES

Abel, P., B. Guenther, R.N. Galimore, and J.W Cooper, 1993: Radiometric gains of satellite sensors of reflected solar radiation: Results from NASA ER-2 aircraft measurements, *IEEE Transactions on Geoscience and Remote Sensing*, **92CH3041-1**, 802-805.

Frouin, R., C. Gautier, and J.J. Morcrette, 1988: Downward longwave irradiance at the ocean's surface from satellite data: Methodology and *in situ* validation. *Journal of Geophysical Research*, **93**, 597-619.

Frouin, R., and R.T. Pinker, 1995: Estimating photosynthetically active radiation at the earth's surface from satellite observations. *Remote Sensing of Environment*, **51**, 98-107.

Frouin, R. and J.J. Simpson, 1995: Radiometric calibration of GOES-7 VISSR solar channels during the GOES Pathfinder benchmark period. *Remote Sensing of the Environment*, **52**, 95-115.

Nielsen, A.A., K. Conradsen, and J.J. Simpson, 1996: Multivariate Alteration Detection (MAD) and MAF post-processing in multispectral, bi-temporal image data: New approaches to change detection studies. Submitted to *Remote Sensing of Environment*.

Pinker, R.T., R. Frouin, and Z. Li, 1995: A review of satellite methods to derive surface short-wave irradiance. *Remote Sensing of Environment*, **51**, 108-124.

Rossow, W.B., Y Desormeaux, C.L. Brest, and A. Walker, 1992: *International Satellite Cloud Climatology Project (ISCCP) Radiance Calibration Report*. WMO/TD-No. 520, WCRP-77, World Meteorological Organization, Geneva, 104 pp.

Simpson, J.J., and C. Humphrey, 1990: An automated cloud screening algorithm for daytime Advanced Very High Resolution Radiometer imagery. *Journal of Geophysical Research*, **95**, 13459-13481.

Simpson, J.J., and S.R. Yhann, 1994: Reduction of noise in AVHRR channel 3 data with minimum distortion. *IEEE Transactions on Geoscience and Remote Sensing*, **32**, 315-328.

Simpson, J.J., J.I. Gobat, and R. Frouin, 1995: Improved destriping of GOES images using finite impulse response filters. *Remote Sensing of the Environment*, **52**, 15-35.

Simpson, J.J. and J.I. Gobat, 1995a: Improved cloud detection in GOES scenes over land. *Remote Sensing of the Environment*, **52**, 36-54.

Simpson, J.J. and J.I. Gobat, 1995b: Improved cloud detection in GOES scenes over the ocean. *Remote Sensing of the Environment*, **52**, 79-94.

Simpson, J.J., and R.H. Keller, 1995: An improved fuzzy logic segmentation of sea ice, clouds and ocean in remotely sensed arctic imagery. *Remote Sensing of the Environment*, **54**, 290-312.

Simpson, J.J. and L. Al-Rawi, 1996: The Tiling and General Research Imaging System (TIGRIS). *IEEE Transactions on Geosciences and Remote Sensing*, **34**, 149-162.

Simpson, J.J. and J.I. Gobat: 1996: Improved cloud detection for daytime AVHRR data over land. *Remote Sensing of the Environment*, **55**, 21-49.

Simpson, J.J., and J.R. Stitt, 1996: A procedure for the detection and removal of cloud shadow from AVHRR data over land. Submitted to *Remote Sensing of the Environment*.

Simpson, J.J., J.R. Stitt, and M. Sienko, 1996a: Improved estimates of the areal extent of snow cover from AVHRR data. To be submitted to *IEEE Transactions on Geoscience and Remote Sensing*.

Simpson, J.J., A. Schmidt, and A. Harris, 1996b: Reduction of clouds in Along Track Scanning Radiometer (ATSR) data over the ocean. To be submitted to *IEEE Transactions on Geoscience and Remote Sensing*.

Simpson, J.J., S.A. Cowley, and R.H. Keller, 1996c: Spatial degradation of satellite data and its effects on accurate cloud detection over the ocean. To be submitted to *Journal of Applied Climatology*.

Whitlock, S. R. Lecroy, and R. J. Wheeler, 1994: *SRB/FIRE Calibration Results and Their Impact on ISCCP.* Proceedings of the AMS 8th Conference on Atmospheric Radiation, 23-28 Jan. 1994, Nashville, Tennessee, 8ATRAD FA 1.1, 4pp.

Yhann, S.R., and J.J. Simpson, 1995: Application of neural networks to AVHRR cloud segmentation. *IEEE Transactions on Geoscience and Remote Sensing*, **33**, 590-604.
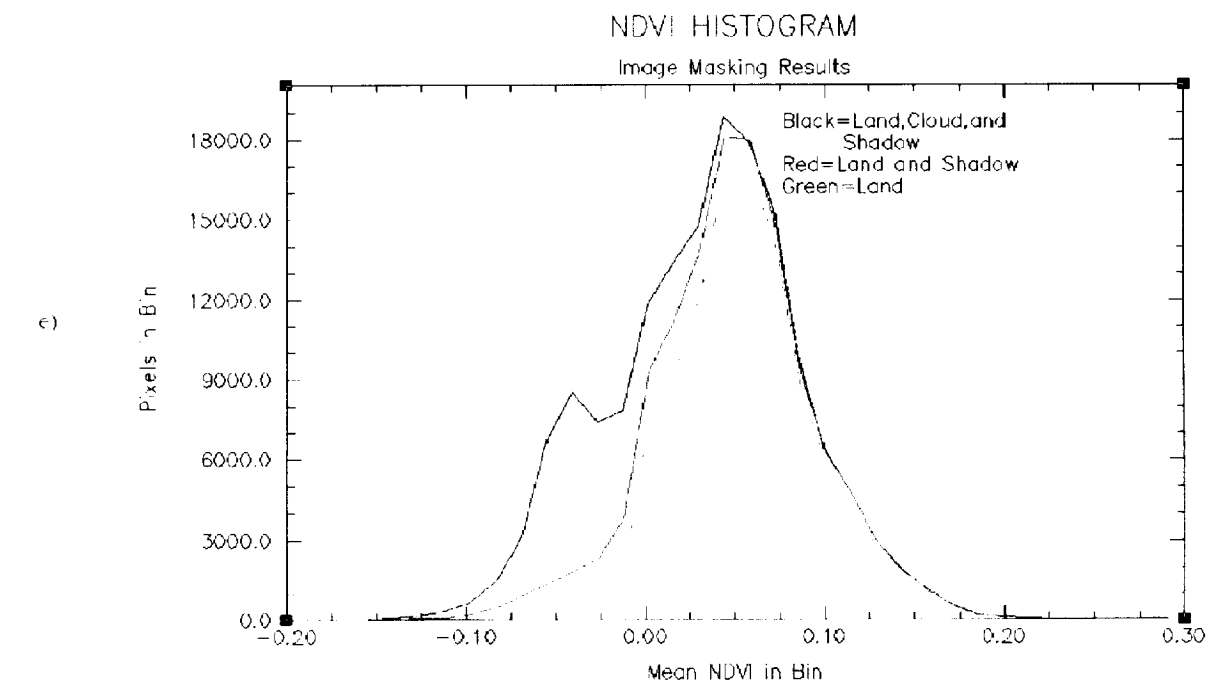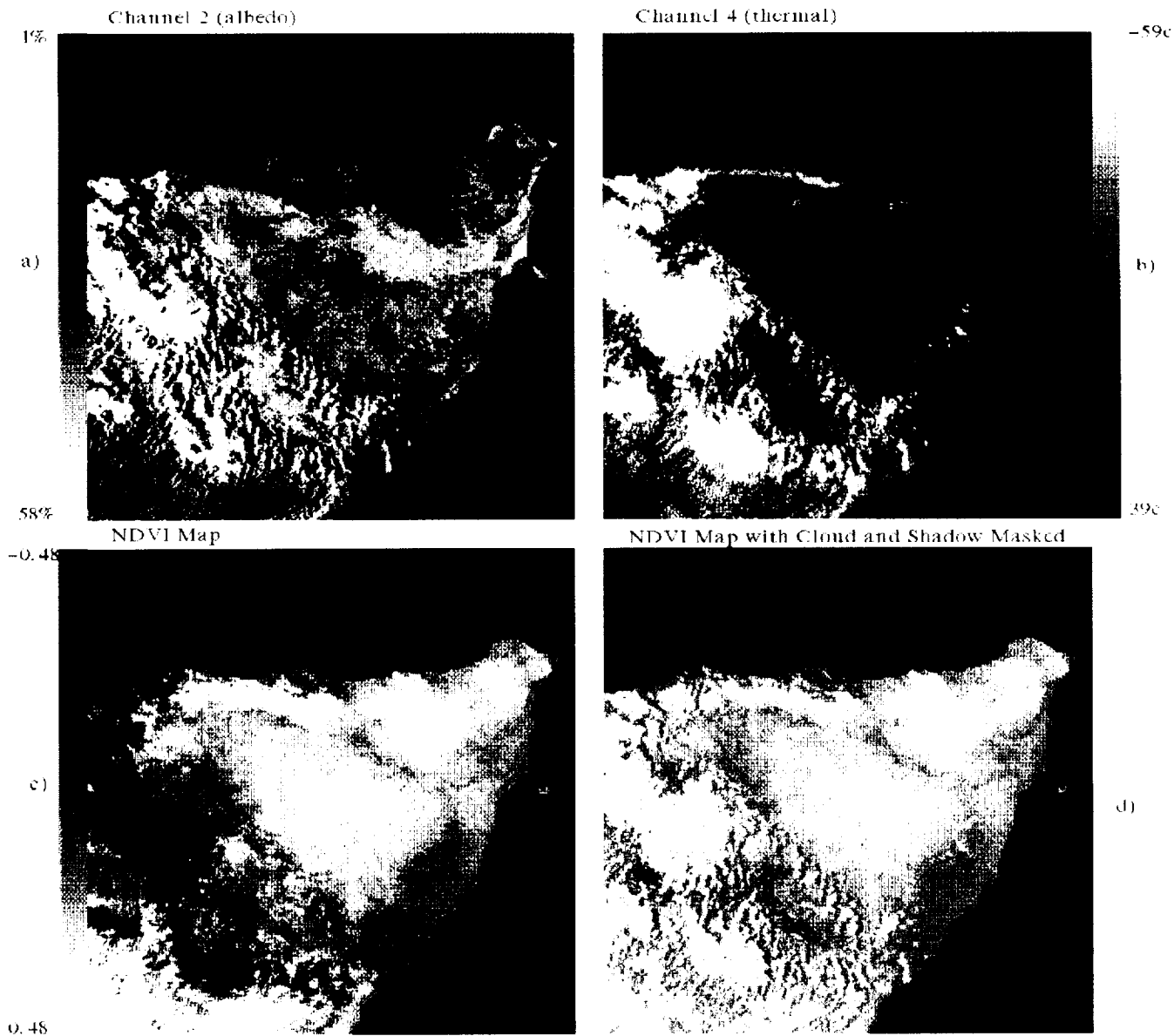
Channel 2 (albedo)

Channel 4 (thermal)

1%

−59c

a)

b)

58%

39c

NDVI Map

NDVI Map with Cloud and Shadow Masked

−0.48

c)

d)

0.48

NDVI HISTOGRAM

Image Masking Results

Black=Land,Cloud,and
Shadow
Red=Land and Shadow
Green=Land

18000.0

15000.0

12000.0

9000.0

6000.0

3000.0

0.0

Pixels in Bin

e)

−0.20   −0.10   0.00   0.10   0.20   0.30

Mean NDVI in Bin

Figure1: High resolution AVHRR scene over Somalia. a) Channel 2 data calibrated to % albedo; b) Channel 4 data calibrated to °C; c) Normalized Difference Vegetation Index (NDVI) ; d) Cloud mask (yellow) produced by ASMC cloud detection algorithm (Simpson and Gobat, 1996) and cloud shadow mask (green) produced using new procedure developed by Simpson and Stitt (1996) ; e) Histogram distribution of uncorrected NDVI scene (black), cloud only removed from NDVI scene (red) and cloud and cloud shadow removed from NDVI scene (green). The changes in the NDVI distribution associated with cloud and cloud shadow removal are important for individual scenes. Use of temporal compositing to cloud screen NDVI scenes will only serve to exacerbate the problems illustrated in this scene.

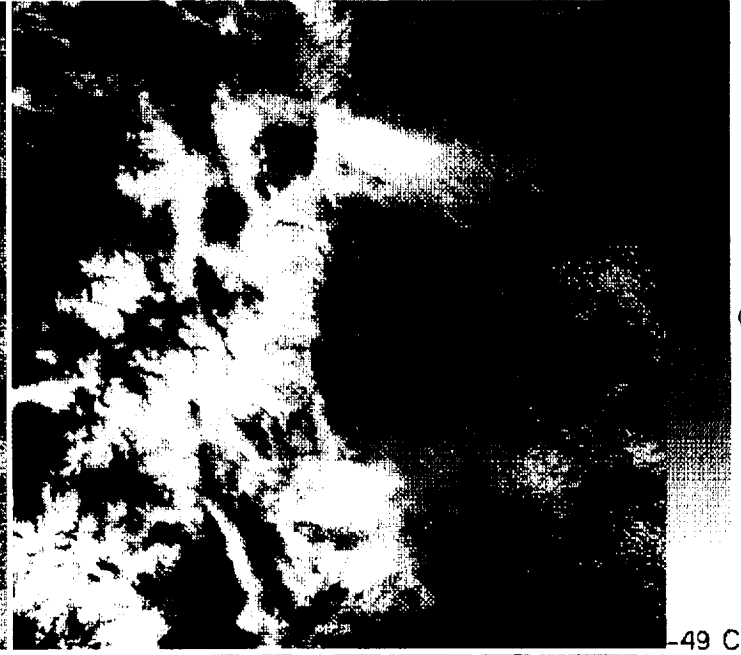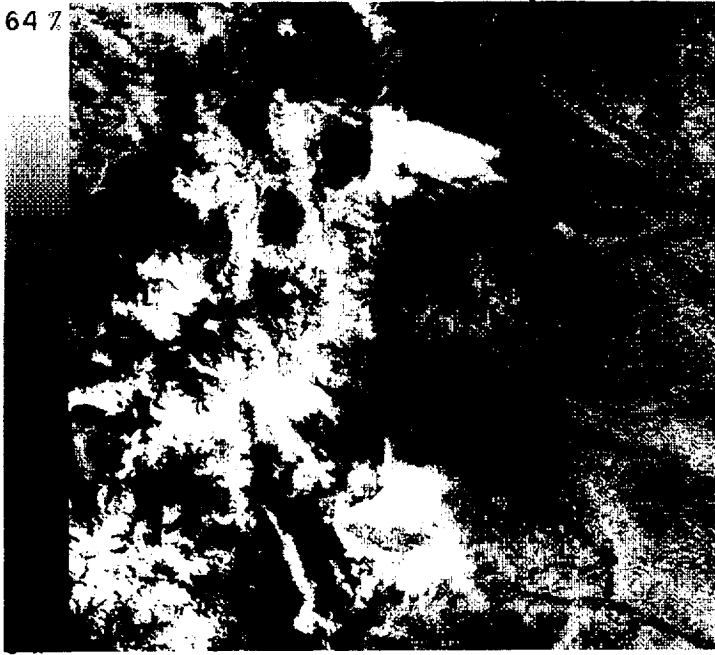Channel 2 (albedo)   Image Reference #: AR7401 Colorado   Channel 4 (thermal)
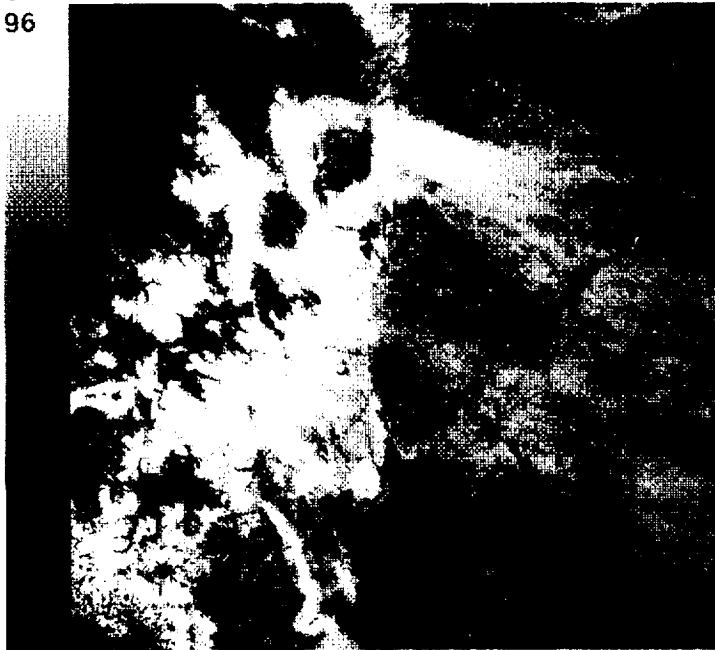
64 %

(a)   (b)

                                                                                  -49 C

96   64 %

(c)   (d)

Reflectance Ratio, R, Used in Stage 1   April 6, 1990   MSSD Classification

Figure 2:   A region over Colorado on March 5, 1984. a) Channel 2 is percent albedo; b) Channel
4 calibrated to °C; c) a new reflectance ratio variable developed by Simpson *et al.*, 1996b; and d)
the new areal extent of snow classification with green for snow, yellow for cloud and purple for
ambiguous where relevant. High albedo, low temperature and high reflectance ratio appear as
lighter shades in panels a, b and c, respectively. Coastlines and lake shores are shown in red and
major water bodies appear blue. The locations of the forty-four SNOTEL sites available for vali-
dation are marked by the white squares (snow), orange squares (clear land) in panel d. Overall
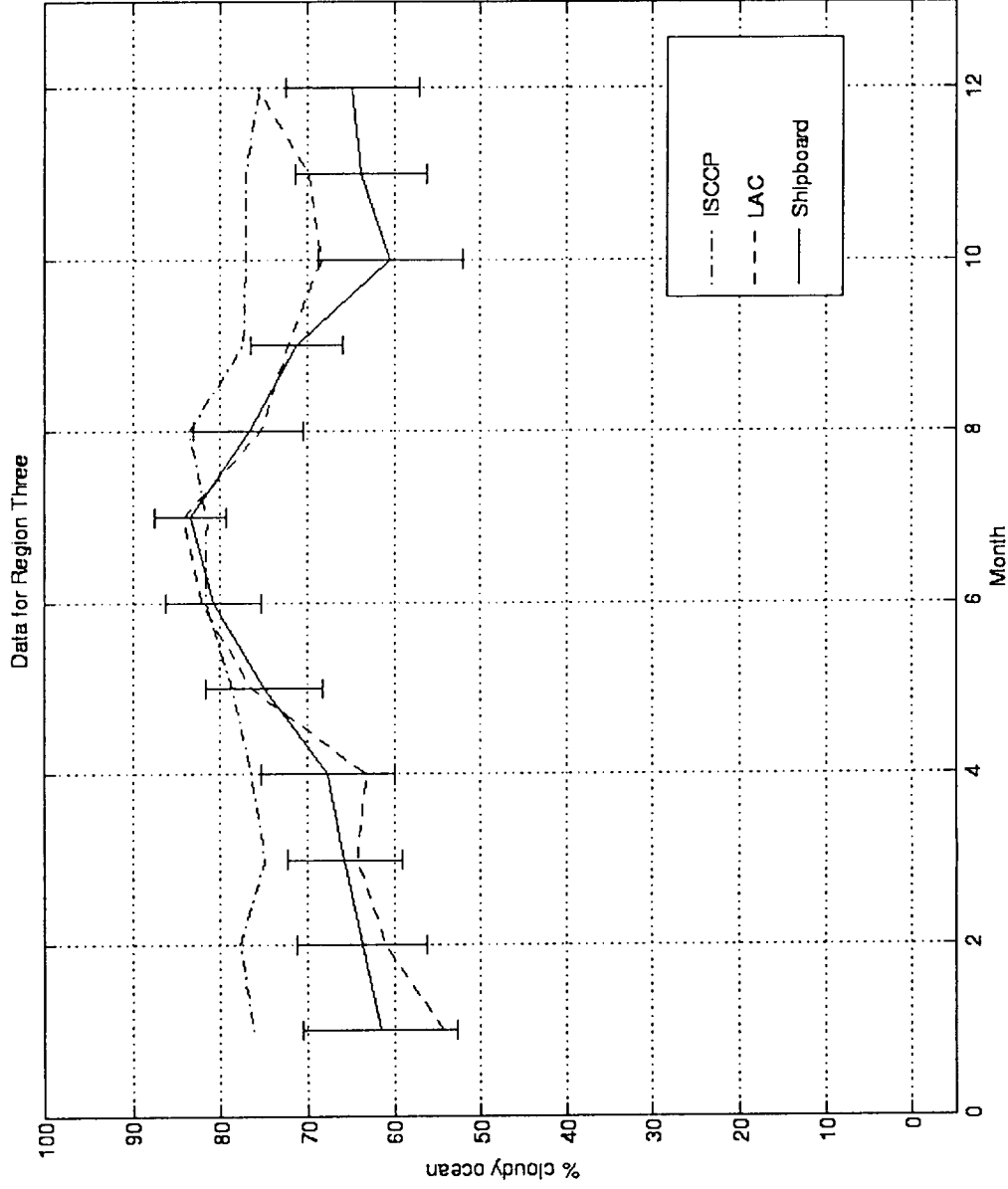classification accuracy on 18 images validated against SNOTEL data was 97.5%

Figure 3 : Comparison of cloud climatologies off southern and Baja California among shipboard data (Nelson and Husby, 1983), estimates from the International Satellite Cloud Climatology Project's (ISCCP) reduced resolution satellite data, and estimates computed by the principal investigator's lab using full resolution (LAC) data. Standard deviation bars also are shown. Between southern California and British Columbia, the variation is similar, except that the mean monthly cloud cover generally is 10 to 15% higher than that off southern and Baja California.

1.6 micron (% reflectance)   Image Reference#: AS12   Date: 02/15/92   View: Forward   11 micron (thermal)

(a)

56 %   −5 C

(c)   (d)

11 C

(e)   (f)

11 C
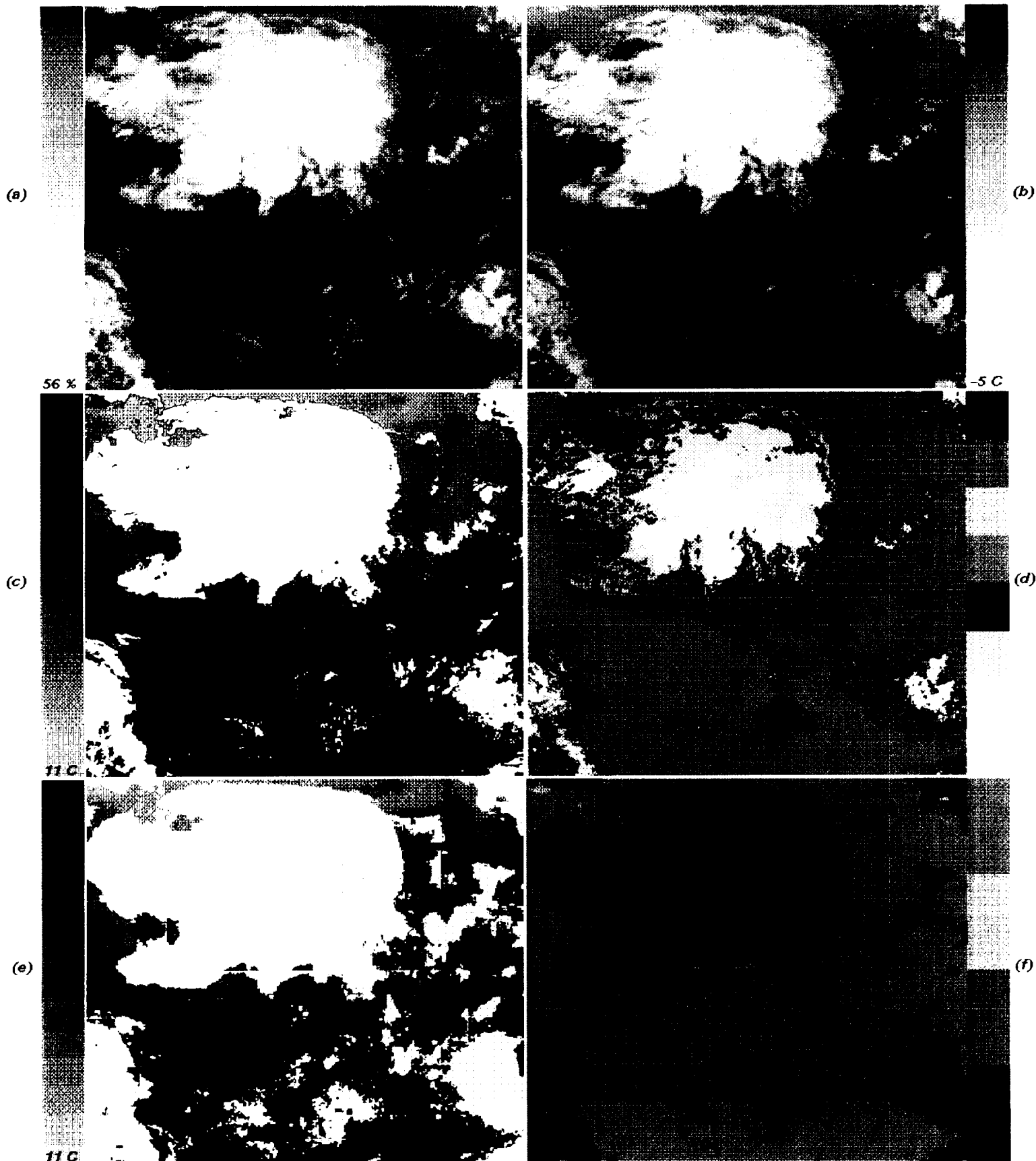
Figure 4:   A scene over a region of the Atlantic Ocean south of South Africa: a) 1.6 μm data scaled to percent reflectance; b) 11 μm temperature data calibrated to °C; c) analogous to panel b but with the basic ATSR/SMC cloud mask (yellow) produced by steps 1-3 of the algorithm and buoy location(s) shown by red circle(s). The effects of the post-processing (step 4, purple; step 5, green; step 6, salmon) are also shown; d) cluster distribution produced by step 2 of the algorithm; e) analogous to panel c but with the SADIST operational cloud mask shown in yellow; and f) Boolean comparison between the two masks: brown both algorithms classify pixel as cloud, purple both algorithms classify pixel as clear ocean, green ATSR/SMC classifies pixel as cloud and SADIST classifies the same pixel as clear ocean; rust is the converse of green. Three buoy observations were available for SST validation.
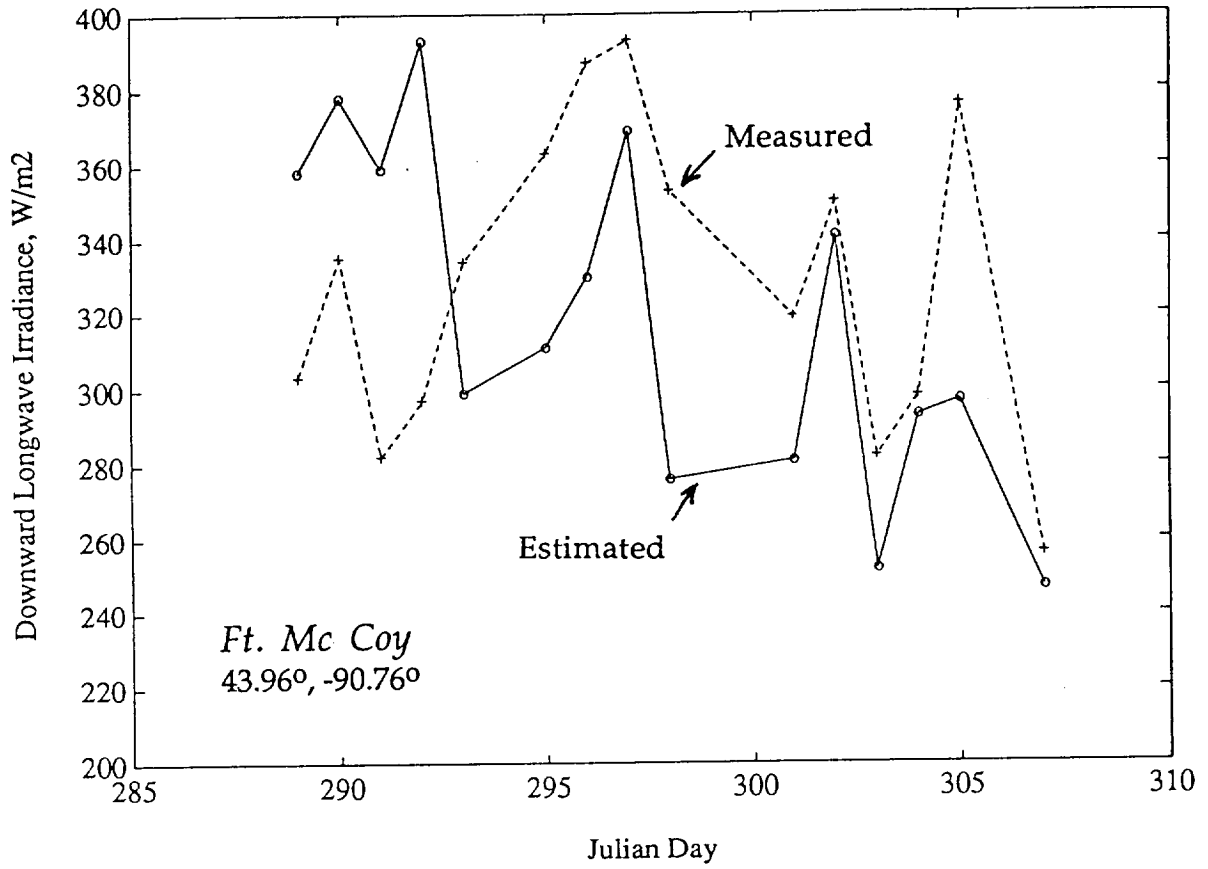
Fig. 5 Time-series of HIRS/2-derived and measured downward longwave irradiance at the surface. HIRS-2-derived values are instantaneous, measured values are 60-minute averages.
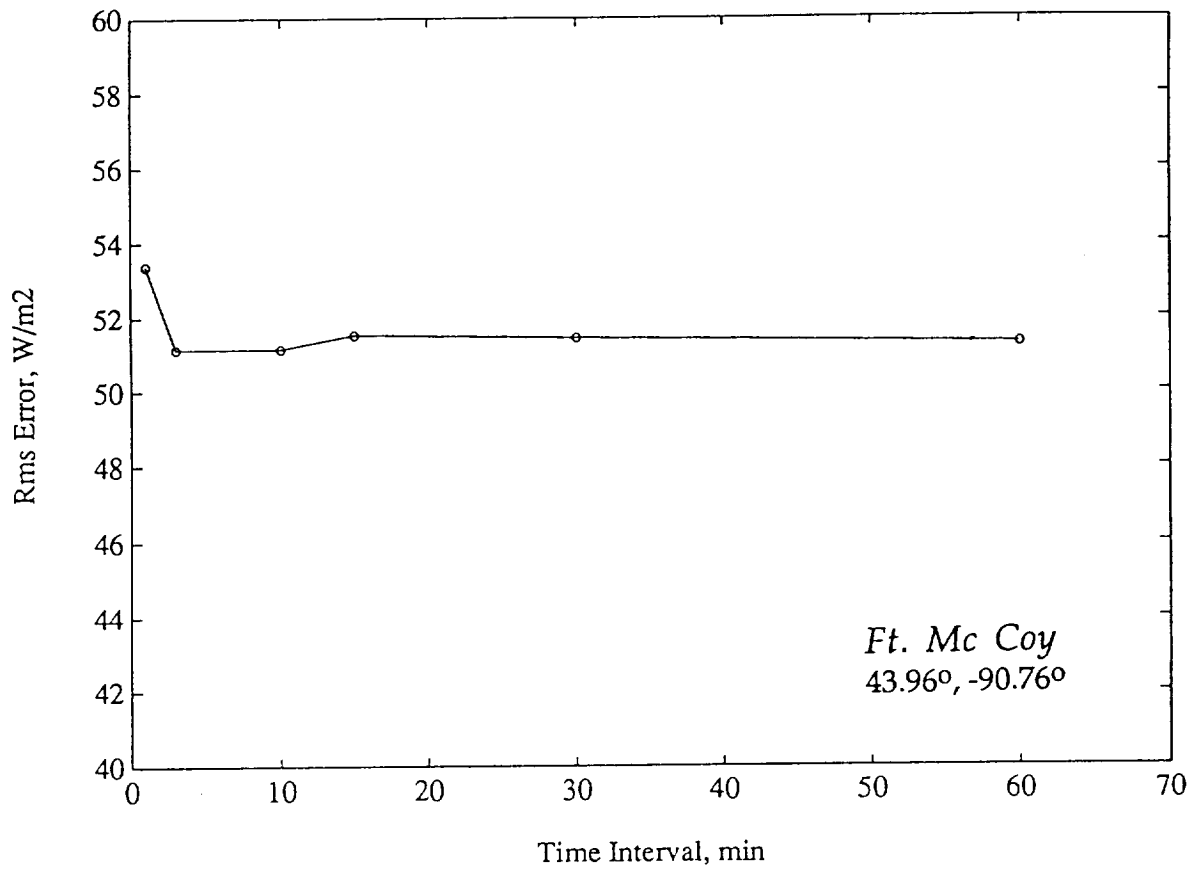
Fig. 6 Effect of time interval used in averages on rms difference.
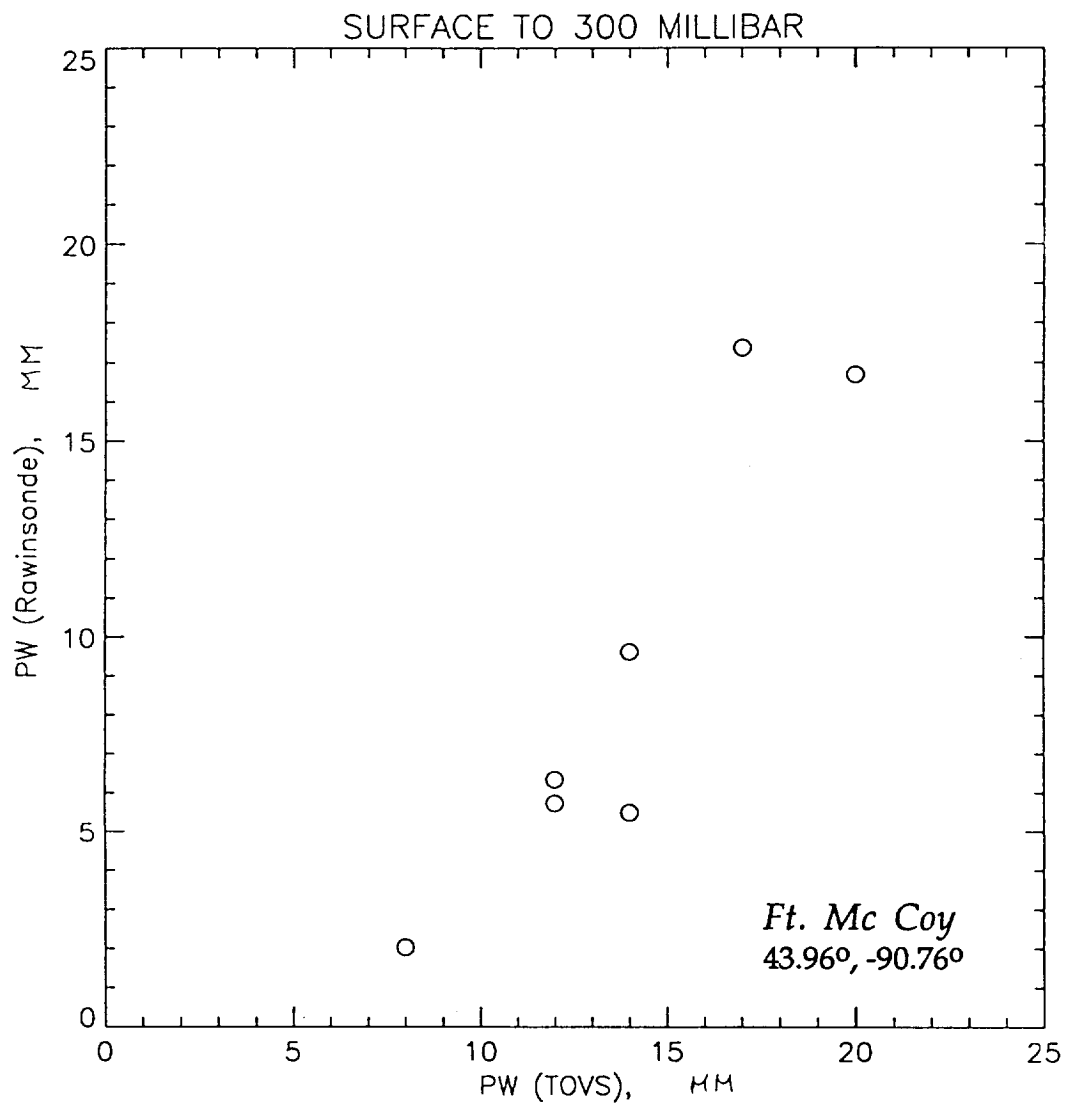
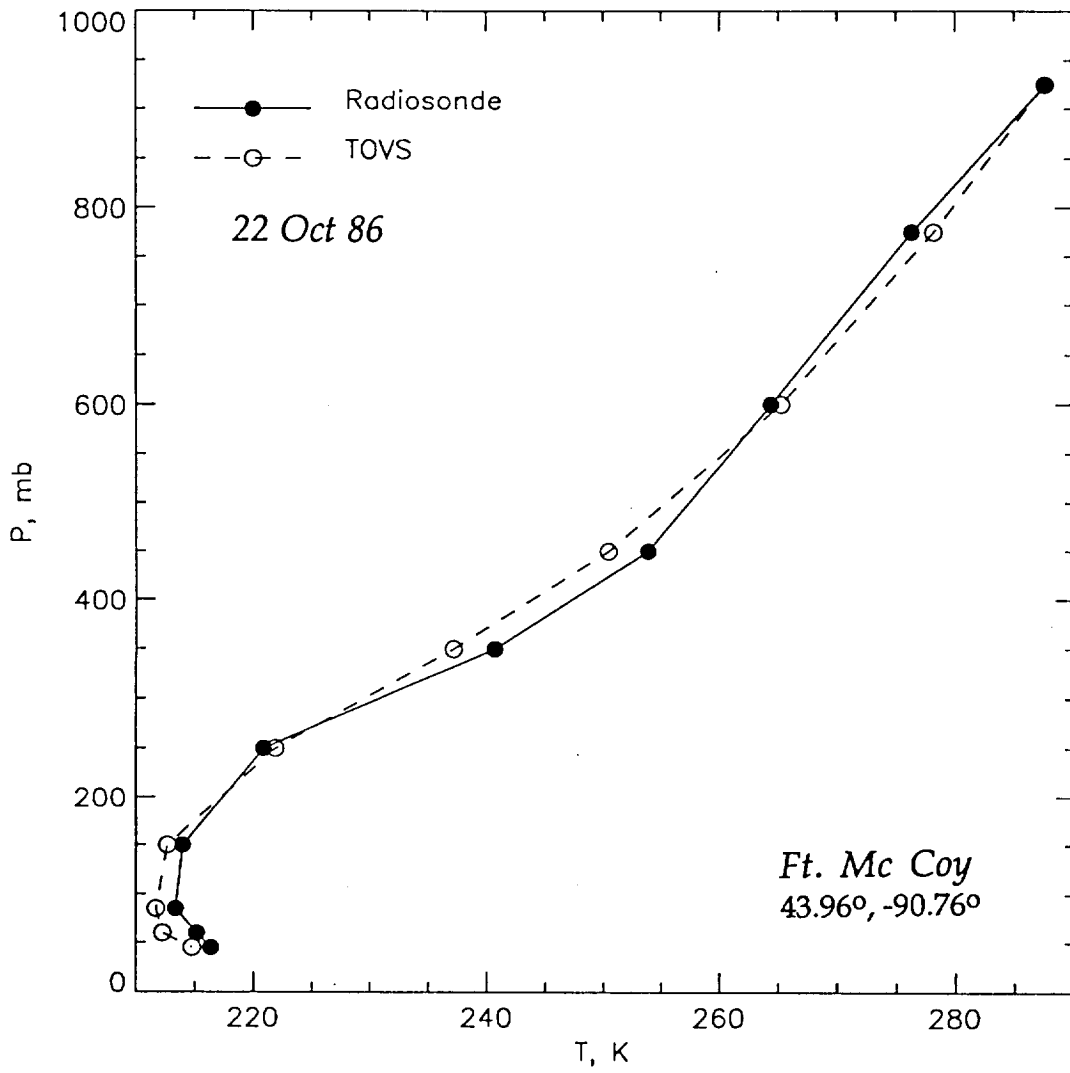Fig. 7 Precipitable water (surface to 300 mb) from rawinsonde and HIRS/2 data.

Fig. 8 Same as Fig. 10, except 10/22/86

Table 1 30-minute average Lidar cloud base versus HIRS/2-derived cloud base at Mc Coy, Wisconsin (43.96°, -90.76°).

Date	Cloud Cover HIRS/2 (percent)	Cloud Base Lidar (km)	Cloud Base HIRS/2 (km)
10/22/86	83	3.8	7.7
10/28/86	93	8.8	6.6
10/30/86	27	9.6	6.2
10/31/86	47	7.5	6.7

Downward Longwave Irradiance, W/m2

AV DIF = 21.3 Wm⁻²
RMS ER = 35.3 Wm⁻²
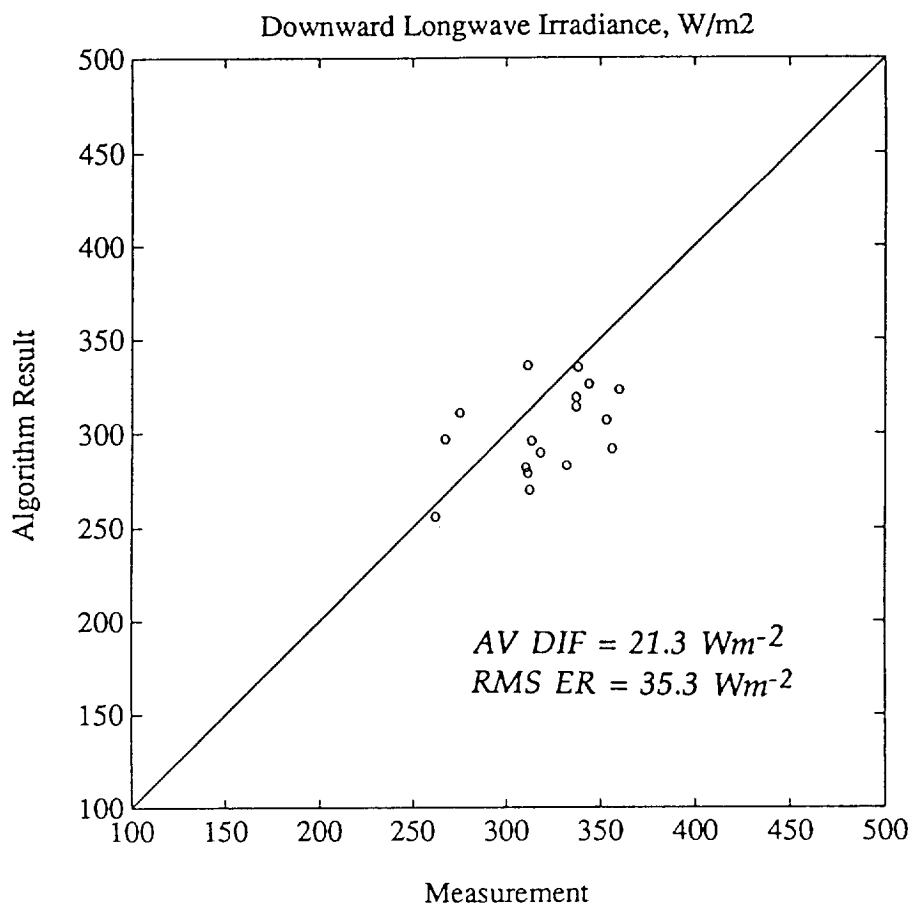
Fig. 9 Algorithm results versus measurements at five surface stations, namely Ft. Mc Coy (43.96°, -90.76), Stevens Point (44.55°, -89.53), Baraboo (43.52°, -89.77°), Adams County (43.97°, 89.80°), and Wautoma (44.04°, -89.30°) for 10/15/86, 10/17/86, 10/22/86, and 10/28/86. Values are daily averages.
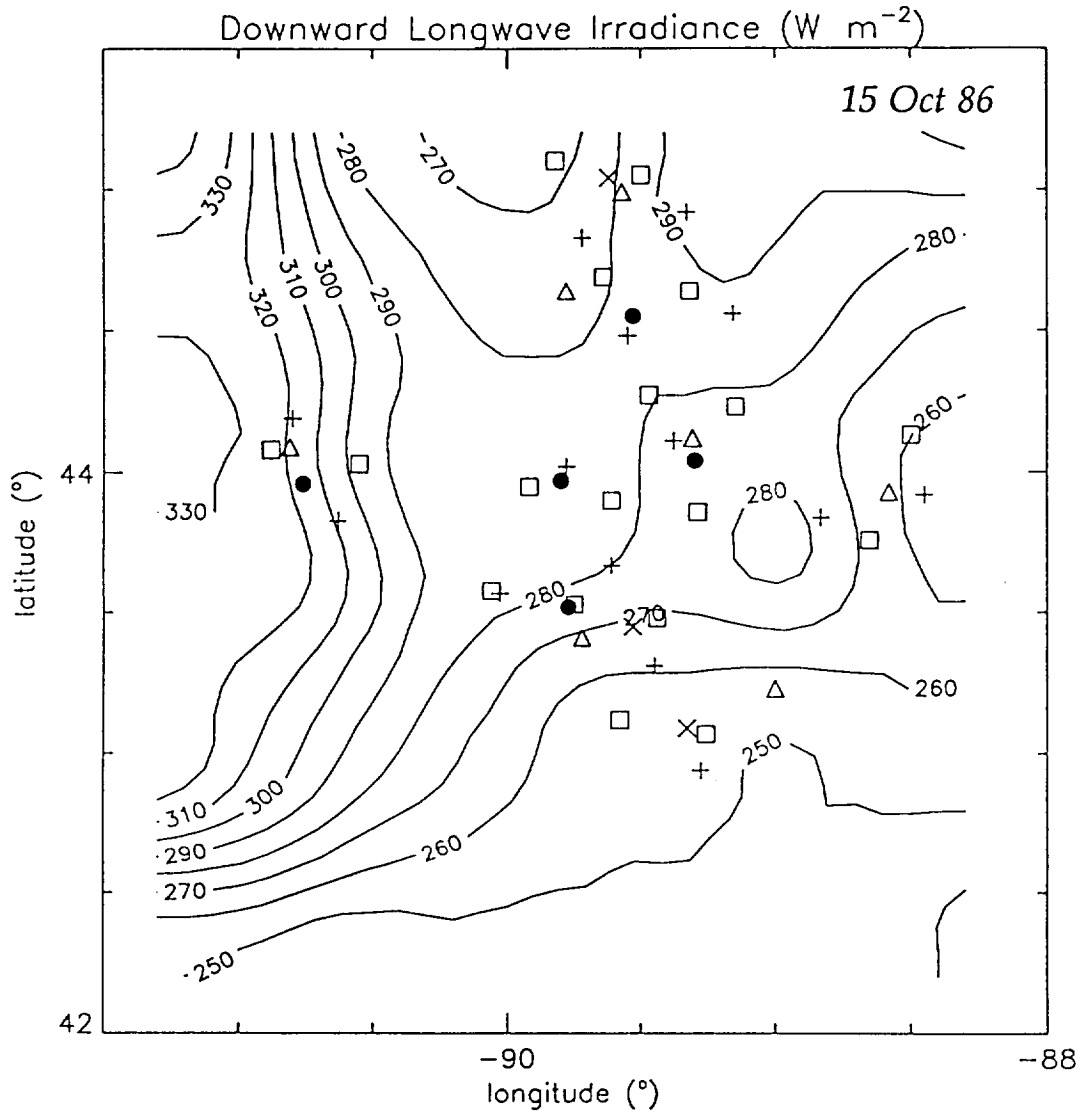
Fig. 10a HIRS/2-derived map of downward longwave irradiance at the surface for 10/15/86.
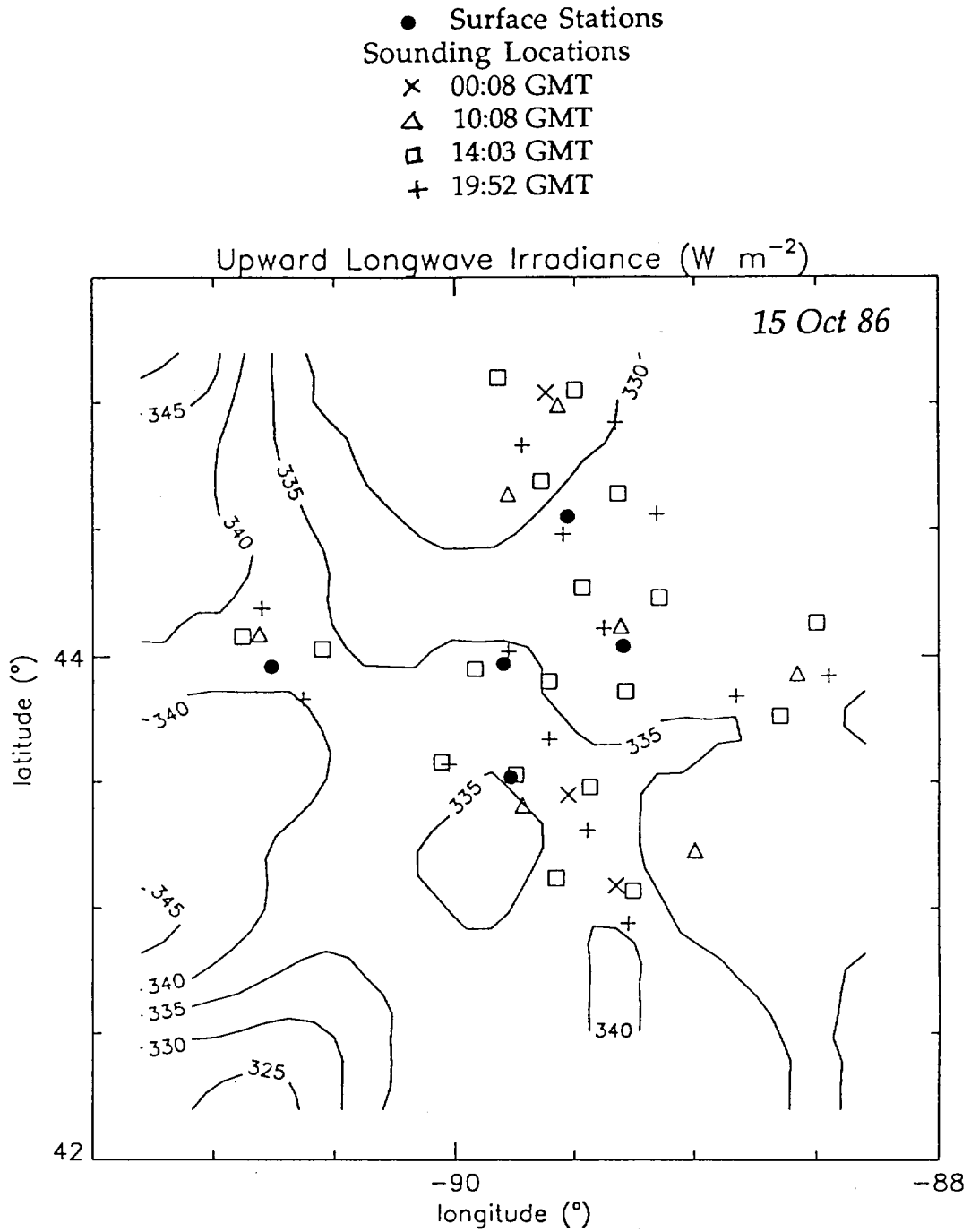
Fig. 10b HIRS/2-derived map of upward longwave irradiance at the surface for 10/15/86.
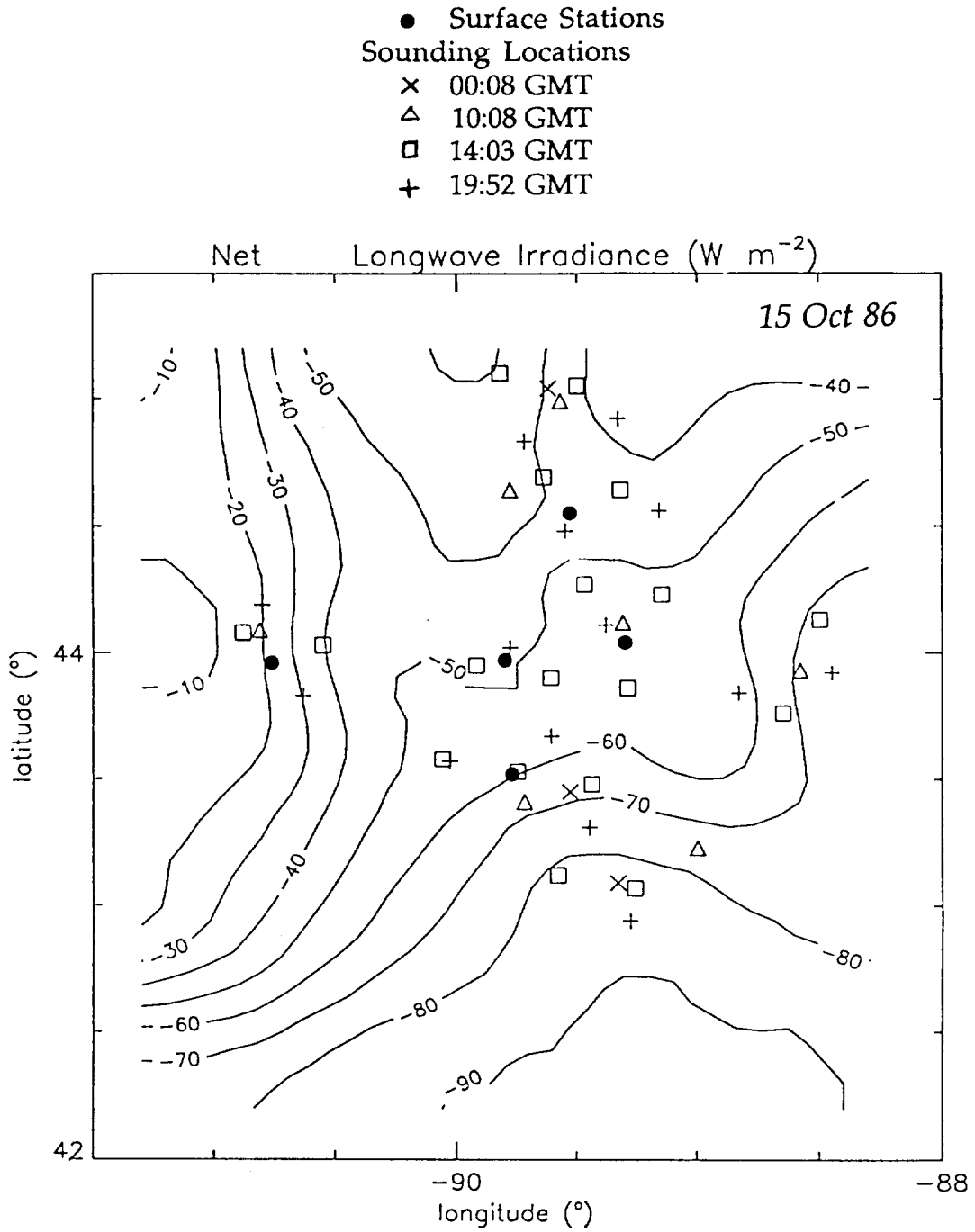
Fig. 10c HIRS/2-derived map of net longwave irradiance at the surface for 10/15/86.